

Popular Summary

Holographic Optical Elements as Scanning Lidar Telescopes

Geary K. Schwemmer

Laboratory for Atmospheres, NASA Goddard Space Flight Center, Greenbelt, Maryland, 20771

Richard D. Rallison

Ralcon, Inc., Paradise, UT 84328

Thomas D. Wilkerson

Utah State University, Logan, Utah 84322-4405

David V. Guerra

Saint Anselm College, Manchester, New Hampshire 03102.

NASA has developed new telescope systems that use holograms instead of lenses or mirrors. These holographic telescopes were developed in an effort to reduce the size, weight and cost of laser instruments used to measure atmospheric properties like temperature and wind. Several hologram designs were made and tested in the laboratory. Two were incorporated into laser remote sensing systems that are used on the ground and in airplanes to study the atmosphere. Our goal is to enable the development of spaceborne scanning laser remote sensors for Earth science applications using the lightest and least costly technologies available.

Holographic Optical Elements as Scanning Lidar Telescopes

Geary K. Schwemmer

Laboratory for Atmospheres, NASA Goddard Space Flight Center, Greenbelt, Maryland, 20771

Richard D. Rallison

Ralcon, Inc., Paradise, UT 84328

Thomas D. Wilkerson

Utah State University, Logan, Utah 84322-4405

David V. Guerra

Saint Anselm College, Manchester, New Hampshire 03102.

We have investigated and developed the use of holographic optical elements (HOE) and holographic transmission gratings for scanning lidar telescopes. By rotating a flat HOE in its own plane with the focal spot on the rotation axis, a very simple and compact conical scanning telescope is possible. We developed and tested transmission and reflection HOEs for use with the first three harmonics of Nd:YAG lasers, and designed, built, and tested two lidar systems based on this technology.

Introduction

Lidar is making significant contributions to those Earth sciences requiring remote measurements of atmospheric and surface parameters from ground-based, airborne, and spaceborne platforms. Scanning provides the means for increasing topographical coverage in airborne laser altimeters, and for generating three-dimensional data sets using ground-based and airborne atmospheric

lidar systems. Scanning will enable high-density global coverage for observing atmospheric dynamic parameters from space, such as cloud and aerosol structure, temperature, and humidity. Of great interest to the atmospheric science community is the possibility for frequent, high vertical resolution, global atmospheric wind profiles. Spaceborne Doppler lidar is currently deemed the most feasible means of obtaining these measurements, and a scanning, pointing, or multiple-look-angle telescope system is required to retrieve full horizontal wind vectors. However, most of the scanning atmospheric lidar systems conceived to date have been too heavy and costly to develop into spaceborne versions. Improvements in efficiency, size and weight are required of all technologies involved in lidar remote sensing in order to realize the advantages over passive sensors that lidar offers, such as high accuracy and vertical resolution. Large improvements may come from developing more efficient laser transmitters, which for atmospheric lidars are usually the heaviest components when the requisite power supplies and radiators are included. The next largest or most massive component is the receiver telescope. Typically, lidars require a large collecting aperture to maximize the laser backscatter signal, and a narrow field-of-view (FOV) to limit the amount of background radiation reaching the detector. In order to scan a conventional lidar system, the entire telescope assembly is steered, or a large flat steering mirror is placed before the telescope to point the FOV in different directions. Focal-plane scanning approaches have been used in altimetry lidars to scan over several degrees, but are generally not viable for atmospheric lidar requiring scans over 90 degrees or more. NASA is investigating a number of innovative telescope technologies, including deployable optics, ultra-lightweight materials, and the use of diffractive optical technologies for various applications. A large reduction in instrument weight can come from utilizing these new optical receiver

technologies individually or in combination, one of which is the holographic scanning telescope described here.

We have developed and experimentally investigated the concept of a scanning telescope using a holographic optical element (HOE) in order to help reduce the satellite resources and costs needed for a large, orbiting laser remote sensing instrument for measuring atmospheric parameters: e.g. wind, temperature, and humidity profiles¹⁻⁴. By rotating an HOE in its own plane, we create a conical scan pattern with a minimum of mechanical and electrical requirements. Used in this manner, the holographic scanning telescope offers advantages over a conventionally scanned telescope in that it reduces complexity and number of parts by substituting a single HOE for the receiver telescope primary optic and the scan mirror. HOEs can be reproduced at low cost compared to large aperture reflectors or refractors. We also investigated using holographic gratings as scanners in conjunction with static HOEs and conventional telescopes, and find special care must be taken to avoid spurious signals from the zero and minus-one orders when these optics are also used to transmit the laser beam.

Review of Scanning Lidars

Scanning lidar systems have been used for a number of applications, using a variety of scanning techniques. Conflicting requirements often arise that tend to drive the scanning system design, with cost usually being a major factor. Most atmospheric lidars utilize large aperture telescopes, which are usually more cost effective and reliable at gaining signal than the use of larger laser transmitters. But the instantaneous FOV (IFOV) of these systems is often very small, usually less than 1 mrad, in order to reduce daytime solar background. There are in general three ways of scanning a telescope with conventional optics. One is to mount the telescope and associated transceiver optics on a scanning mount. Such mounts are relatively large and expensive in order

to accommodate the mass and inertia of the telescope assembly. Astronomical telescopes and tracking mounts are examples of this type. An early example of a lidar employing this type of scanning is the Large Atmospheric Multi-Purpose lidar⁵. More recently is the design proposed for what would have been the first scanning spaceborne lidar, the Atmospheric Lidar Instrument⁶, but that has since been changed to a non-scanning system.

The second type of scanning telescope utilizes one or more large flat scanning optics in front of the telescope aperture. An example using one mirror mounted on a single-axis scanning mount is the Goddard Scanning Raman Lidar⁷. Another example of this type is the lidar mounted on the NASA DC-8 during the SUCCESS campaign⁸ in which the scan mirror was mounted within a pod on the outside of the aircraft's fuselage. Hwang's lidar terrain mapper system⁹ also uses a single rotating flat scan mirror to achieve cross-track coverage from an airborne platform. Some systems are designed with a single flat mirror on a two-axis mount. This allows for somewhat more flexibility, including 3-dimensional volume imaging at the expense of a more limited scan-angle range, and requires a somewhat larger flat mirror. The Large Aperture Scanning Airborne Lidar¹⁰ uses a two-axis scanning mirror in front of a 55 cm diameter telescope situated in the bomb bay of the NASA P-3B aircraft. The telescope is mounted horizontally, pointing aft at the scan mirror. The scan mirror is nominally tipped at 45 degrees and rotates ± 45 degrees on a shaft aligned with the telescope optic axis to effect cross-track scanning. A big disadvantage of this arrangement is the large scanning flat mirror is not only heavy, but requires a large motor and gearbox to achieve the torque required to constantly accelerate and de-accelerate the mirror. In addition, since the scanning mirror is within the confines of the fuselage, a large open area is required to permit an unobstructed 90-degree cross-track scan, achieved in the P-3B by removing the bomb bay doors. Other examples of lidars using single 2-axis scanning flats include those of

Irish and Lillycrop¹¹, Hawley et. al.¹², and Bennett et. al.¹³. Sometimes refractive rotating wedges are used instead of mirrors to generate a conical scan in a more compact design. The Wind Infrared Doppler Lidar¹⁴ is one example of a system using a rotating germanium wedge to scan its infrared transceiver telescope. Similarly, the Multi-center Airborne Coherent Atmospheric Wind Sensor¹⁵ used two rotating wedges to steer the IFOV over any direction within a limited total angular range. The majority of 2-axis scanning lidars utilize two flat mirrors each on its own single-axis mount, in an azimuth – elevation scan configuration. This usually allows for complete hemispherical coverage in ground-based systems, but is awkward and expensive to incorporate into airborne systems and would be prohibitively large and heavy for spaceborne use. Example lidars with two scan mirrors are the University of Wisconsin's Volume Imaging Lidar¹⁶, the system of Hooper and Martin¹⁷, the Raman water vapor lidar of Eichinger et. al.¹⁸, and the Goddard Lidar Observatory for Winds¹⁹. Occasionally rotating polygon mirrors are used for rapid scanning in one axis, but these systems are limited in size to smaller apertures and are usually applied in terrain mapping or other hard-target lidars such as the one described by Chen and Ni²⁰.

The third major category of scanning lidar telescope using geometric (conventional) optics involves focal-plane scanning mechanisms. These systems utilize either a small scanning mirror in the focal plane, or an array of detectors combined with separate transmitter beam steering optics. This type of scanning requires a telescope with a total FOV as wide as the angular extent of the scan. This appreciably adds to the cost of a large telescope when the scan angles are greater than a few degrees and is generally limited to altimeters and similar hard-target lidars. The Laser Vegetation Imaging Sensor²¹ is one example of an airborne scanning lidar that uses a

small oscillating galvanometer scan mirror in the focal plane, coupled with a wide FOV telescope, to achieve ± 7.5 degree cross track scanning.

Holographic Optical Elements

An HOE can be thought of as a hologram of a point. It is constructed using the fringe pattern generated by the interference between two beams of mutually coherent monochromatic light. (Fig. 1a) One beam (called the object beam) is from a point source and has spherical wavefront. The other (called the reference beam) is collimated, having a planar wavefront. After exposing and processing is complete, one can “play back” or reconstruct the recorded image of the point source by illuminating the HOE with light from a collimated or quasi-collimated source conjugate (in the opposite direction) to the original reference beam (Fig. 1b). The fact that it can be illuminated simultaneously by light from many such reference beams such as from a distant extended source or object, each reconstructing a corresponding point in the image plane, gives the HOE lens-like imaging properties. We refer the reader to Close²² for a basic treatment of HOE formation, imaging and dispersion properties, including a comparison with conventional imaging optics. In addition to acting as a telescope’s light collecting objective, the HOE can also be used to transmit the laser beam in a lidar system, collimating and steering it at the same time.

The use of HOEs for scanning lasers is not new, nor is the idea of using one as a lidar telescope. Rallison²³ conceived of using a static HOE as a spectrally discriminating collecting telescope in a laser range finder. Gilbreath et. al.²⁴ discussed using HOEs as lightweight transceiver optics for collimating and correcting astigmatism in diode laser transmitters for spacecraft optical communication systems. The use of HOEs in laser beam scanners for optical bar code readers is commonplace, with many patents existing in this area. However, most such previous rotating scanners attempt to straighten out the path of the scanned beam, which would

otherwise describe a circle. These systems use small pie-shaped segments of the scanner, each containing a separate HOE to scan the beam at different angles. This makes for very inefficient use of the available aperture, which is the opposite design feature required by typical lidar systems, where the weakness of the return signals necessitates the use of large photon collecting apertures.

The first HOE we designed and constructed to use with a conical scanning lidar was a 40 cm reflection hologram for use with a 532 nm wavelength laser¹. It was tested in the laboratory and in a breadboard lidar system before being incorporated into what is now the Prototype Holographic Atmospheric Scanner for Environmental Remote Sensing (PHASERS)²⁵, and discussed in more detail later in this paper. Encouraged by the successful demonstration of our concept, we proceeded to develop HOEs for use with other laser wavelengths^{26, 27} and applications. This led to development of the Holographic Airborne Rotating Lidar Instrument Experiment (HARLIE) based on a transmission HOE for use with the 1064 nm wavelength of the Nd:YAG laser²⁸. The use of a transmission HOE allows the system to scan over wide angles through a similarly sized window in the aircraft. We are currently developing holographic telescopes for use with UV (355 nm) wavelengths, 1-meter diameter apertures, and as dispersive optics for Raman lidar applications²⁹. We are also investigating further reduction in mass by eliminating all moving parts^{30, 31} using angle multiplexed HOEs.

In the remainder of this manuscript we describe the manufacturing and optical testing of the HOEs used in our work. We give a short description of the two holographic scanning lidars we have developed. We then discuss several practical aspects of using HOEs in lidar receivers before concluding.

Fabrication of HOEs

For our purposes HOEs can be divided into two categories: *reflection HOEs*, in which the incident and diffracted light are on the same side of the HOE, and *transmission HOEs*, in which incident and diffracted light are on opposite sides of the film. We investigated both reflection and transmission HOEs in this program.

Reflection HOEs have the advantage of being able to utilize opaque substrates to support the holographic film or pattern, which opens the possibility of being able to use ultra-lightweight materials such as graphite epoxies and similar composites. Volume phase reflection HOEs must be produced on transmissive optical substrates and may be applied to opaque substrates using film transfer techniques, although these techniques have not been developed for large ($\sim >10$ cm) holograms. However, reflection HOEs can also be produced as surface relief holograms using reactive ion etching or other techniques directly to an opaque substrate. Reflective coatings can be applied to boost the diffraction efficiency.

Transmission HOEs must be applied to optically transmissive substrates such as glass. They are well suited for airborne systems in which one is restricted to having the instrument view through a pressure-sealed window. Placing the receiver HOE very close to the window minimizes the size of window needed to accommodate the wide scan angle. The Bragg planes in reflection HOEs tend to be oriented at oblique angles relative to the optic axis, whereas in transmission HOEs they tend to be oriented at acute angles with respect to the optic axis (which is normal to the film in our examples). Due to this aspect of the fringe-plane structure in transmission HOEs, it is also easier to reduce aberrations to the image quality, allowing one to use a smaller FOV to help decrease daytime solar background levels in lidar telescope applications.

We first produce a master HOE from which working copies are made. The master is produced by exposing a glass plate coated with a film of dichromated gelatin (DCG) emulsion to two mutually coherent laser beams as illustrated in Fig. 1a. Molecular cross-links are formed in the gelatin upon exposure to light, thus the interference fringes are registered in the film as variations in hardness and index of refraction. Post-exposure processing is performed on the film by alternately immersing the film in water to remove the photosensitive dichromate from the gelatin and hot isopropyl alcohol to remove the water. The resulting hologram is then relatively free of absorption. The HOE is then oven dried and tuned if necessary to adjust the peak response wavelength by adjusting the water content of one of the alcohol processing baths and reprocessing the plate. Adjusting the water content causes the film to shrink or swell in thickness, thereby changing the tilt and modulation of the fringe planes and hence the center wavelength and efficiency at the correct diffraction angle. The HOE focal spot size is checked, and if within specification the film is hermetically sealed with a cover glass cemented to the film side of the substrate and sealed around the edges with UV curing epoxy. The spot size is rechecked, and if it is still acceptable, an anti-reflection (AR) coated cover glass is epoxied to the original uncoated cover glass. Since many trials are often required to produce a satisfactory master HOE, the AR coated glass is not used throughout this process due to cost considerations.

The development of the first HOE for practical atmospheric lidar applications faced the challenge of making a large (40 cm) diameter optic having both high diffraction efficiency and a small focal spot size. This had to be done using a relatively short focal length in order to design a receiver system compact enough to be competitive with conventional Cassegrain telescopes typically used in lidar receivers. The final design choice was an $f/3.2$ reflection HOE for use at 532 nm.

The second major step to eventual spaceborne use was developing an airborne lidar system to not only demonstrate the HOE technology, but would also have scientific utility. We wanted to work at the Nd:YAG laser fundamental at 1064.7 nm to measure atmospheric aerosol backscatter. DCG is non-absorbing at this wavelength. The only suitable laser available for exposing this hologram was a 488 nm Argon ion laser. At the same time we wanted to decrease the focal spot size in order to be able to utilize the HOE in a lidar system having daytime capability with the small laser pulse energies produced by a diode-pumped Nd:YAG laser. Spherical and other aberrations can increase dramatically when a hologram is played back at a wavelength well removed from the exposure wavelength. A number of approaches were considered and tried in developing an HOE that would work well at 1064 nm when exposed at 488 nm. The final approach that met with great success was the method of "time-reverse ray tracing"²⁶. Once this technique was perfected, the designs for several transmission HOEs were developed and built in rapid fashion for a variety of lidar applications that would employ 770, 1046, 832, 523, and 532 nm light.

In general, the HOEs were fabricated on Solarphire or B270 float glass that was spin coated with 10-micron thick films of DCG. Several copies of each design were exposed, processed and tested. The best device in each case, in terms of focal spot size, was capped with an AR coated Solarphire cover and used as a master from which contact copies were made. The masters were made to diffract about 50% when illuminated with 488 nm light. Contact copies were produced by placing the master HOE in close contact over a glass substrate coated with a fresh layer of unexposed film and its intended cover glass. Index matching xylene is forced and held between the three pieces by capillary action. A laser beam sheet was produced with cylindrical and spherical lenses, then reflected 90 degrees off a long, narrow flat mirror on a mount moving

parallel to the HOE to scan the master /copy film (Fig. 2). The scanning laser light passes through the master HOE to the unexposed film. A portion of the light is diffracted into the first order, forming a collimated sheet traveling at an angle with respect to the undiffracted beam with which it interferes to produce the fringes that will expose the copy film. Because the distances between the interfering wavefronts are short, the coherence length of the laser used to make the copies need not be as great as that making the original. And because the laser light is only formed into a sheet rather than a fully collimated beam, the intensity per unit area is greatly increased, greatly decreasing the required exposure time for any given portion of the film. For these reasons, the scanning mirror can be moved at a moderate pace and does not require interferometric stability.

Several of the HOEs and holographic grating scanners made during the course of this research are pictured in Fig. 3. Clockwise from the left foreground: A 25 cm transmission grating for use at 1046 nm, a 40 cm transmission HOE for 1064 nm, having a 100 cm focal length and 45 degree diffraction angle; a 40 cm tiled mosaic transmission grating optimized for 770 nm at 45 degrees. This optic was made in four exposures (one in each quadrant) to demonstrate one method of scaling the manufacturing process to meter sizes. The hole in the center is for transmitting a high power Q-switched YAG laser beam, which would be steered in the proper direction with a prism mounted in the hole and rotating with the grating. To the right is a 30 cm reflection HOE for 532 nm light at 45 degrees, and in the front center is a 20 cm transmission grating similar to item #1. Notice the diffracted image of the coffee mug just to the right of the mug placed behind the hologram. In the lidar, we transmit the outgoing laser light through a concave lens f-matched to the HOE, which then collimates the light while diffracting it at an angle to the substrate. Laser light backscattered by the atmosphere acts as the reconstruction

beam and is focused on the center normal to the HOE. Spinning the HOE about the center normal axis generates a conical scan with the transmitted light and the receiver FOV (Fig. 4). Components from the field stop to the detector remain fixed so no slip rings are required. This makes for a simple compact design.

Optical Performance

Being diffractive, HOEs are spectrally dispersive. The dispersion is determined by the surface grating defined by the intersection of the Bragg planes with the surface of the film and is given by the well known grating equation:

$$\sin \alpha + \sin \beta = m\lambda/d, \quad \text{Eq. 1}$$

where α is the input angle, β is the output angle, m the diffraction order number, λ the wavelength of the light used to "playback" the hologram, and d is the surface spacing of the Bragg-plane fringes. To rotate the HOE in its own plane and keep the focus on a fixed point, the angle β must be 0° . Spectral dispersion helps to filter out background light, since the light at undesired wavelengths is dispersed in the focal plane and will fail to enter the field stop aperture. However, light from different parts of the sky at other wavelengths (within the bandpass of the HOE) will be diffracted into the field stop.

The spectral bandwidth $\Delta\lambda$ for a transmission HOE designed for use at a wavelength λ is

$$\Delta\lambda \approx \lambda d / T \tan \phi, \quad \text{Eq. 2}$$

and for a reflection HOE is

$$\Delta\lambda \approx \lambda d / T, \quad \text{Eq. 3}$$

where $\phi = |\alpha_n + \beta_n|/2$ is the diffraction half-angle, the subscript n denotes angles inside the film, and T is the thickness of the film.

The expected efficiency η , of a transmission HOE is given by

$$\eta \approx \sin^2[\pi \Delta n T / \lambda \cos \phi], \quad \text{Eq. 4}$$

and for a reflection HOE by

$$\eta \approx \tanh^2[\pi \Delta n T / \lambda \cos \phi], \quad \text{Eq. 5}$$

where Δn is the peak-to-peak index modulation (the difference between the extremes in index of refraction values in the fringes).³²

For example, using $\lambda=532$ nm, a typical film thickness of 10 μm , refractive index 1.27, $\Delta n=0.03$, $\alpha=45^\circ$, and $\beta=0^\circ$, a transmission HOE will have a peak diffraction efficiency of 89%, and a bandwidth of about 132 nm. Similarly, a reflection HOE with similar parameters will have a peak efficiency of 53% and a bandwidth of 40 nm. The amount of light diffracted as a function of wavelength was measured for the first 532 nm reflection HOE, using a high pressure Mercury arc lamp at the focus of a collimating parabolic mirror to illuminate the HOE (Fig. 5). The peak response (uncorrected for lamp output) occurs around 528 nm and the spectral bandwidth (FWHM) is about 46 nm, within 15% of the expected value. Frequently, bandwidths calculated using Eqs. 2 and 3 do not agree this well with actual bandwidths, because of gradients and chirp in the actual diffractive structure in the HOE. Depending on how a plate is processed, it may play back as if it had 40-80% of the original film thickness because most of the modulation is in the top few microns and not evenly distributed throughout.

Table 1 lists the various HOEs and gratings that were designed, fabricated, and tested as part of this program. Item #1R is the PHASERS reflection HOE made in 1989, described earlier in this paper. Item #2 is a prototype to the HARLIE HOE. Items #3-5 are transmission gratings conceived for use with existing lidars having conventional telescopes. Using improved fabrication techniques developed during this program, #6R was made in an attempt to improve on the efficiency and angular resolution of #1R. Its incident angle was designed to be 43 degrees to match the actual diffraction angle of #1R, in order to replace it in the PHASERS system without having to make any mechanical changes to the lidar. Items 7a, 7b, 8a, and 8b are designed to be used in pairs for Nd:YLF-based terrain mapping lidars. The a's are transmission gratings that rotate to perform the scanning function, and the b's are transmission HOEs with the collimated beam normal to the optic and the focus off-normal.

We tested the HOEs at their design wavelengths for focal spot size, diffraction angle, efficiency, and focal length using a horizontal collimated beam of laser light at the appropriate playback wavelength, expanded to fill the diameter of the HOE (Fig.6). To correctly orient an HOE to the collimated beam, first the tilt about a horizontal axis along a diameter of the HOE is adjusted so that the specular reflection from its front surface will remain in the horizontal plane. The front surface is identified during manufacturing as the side that a collimated light source should impinge upon to create a focused spot by diffraction. The HOE is then aligned about a vertical rotation axis (also a diameter of the HOE) while monitoring the focal spot with a CCD camera, to give the minimum spot size. The HOE is then rotated in its own plane to bring the focal spot into the horizontal plane. Then the vertical rotation angle is readjusted to minimize the spot size. This establishes the proper incidence angle of the collimated beam with the HOE and the plane of diffraction. We usually find small differences between the incident angle that

produces the smallest focal spot and the incident angle that produces the highest diffraction efficiency, but this is usually less than a degree. It is a matter of judgment exactly which angle to use. The spot size is more sensitive than efficiency to departures from the optimum incidence angle, efficiency only changing by 1 or 2 percent over a few degrees. So the optimum angle is the one that produces the smallest spot (Fig. 7). The plane gratings were tested only for diffraction efficiency and diffraction angle.

Diffraction Efficiency

To test the diffraction efficiency of each of the holograms we measured the total energy incident on the HOE and the energy in the first-order diffracted spot. The measurement of the light incident on the HOE was made using a Fresnel lens to collect the light from over the full aperture and focus it onto a 1 cm² power meter, as shown in Fig. 6. The same Fresnel lens and meter were then placed on the opposite side of the HOE to measure the diffracted power. We divided the diffracted power measurement by the incident power measurement to calculate the first-order diffraction efficiency. We also measured the zero-order (undiffracted) transmission in this fashion. The test data for the HOEs listed in Table 1 are recorded in Table 2. The percentages in the zero and first orders do not add up to 100 % because some light is lost to scattering, absorption, Fresnel reflections, and other diffraction orders. Item #7a was also tested at 904 nm to see how it might perform if used with a diode laser altimeter system at that wavelength.

The focal lengths were measured with calipers and a ruler from the focal point to the center point of the surface of each HOE.

The diffraction angle for each grating was measured directly, by retro-reflecting the first order light with a large, flat mirror, and then measuring the difference in angle between the flat mirror and the HOE with a theodolite (Fig. 8).

Different methods were used to measure the diffraction angles of the HOEs. If the HOE was designed with the collimated beam off-normal, the incident angle was measured using the theodolite in a manner similar to the gratings. If the HOE was designed with the collimated beam normal and the focus off-normal, the diffraction angle of the focus-side optical axis was calculated geometrically using measurements of the focal length and its displacement from the central normal ray.

Spot Size

The focal spot size of each HOE was measured with a CCD camera set in the focal plane of the HOE's. The focal spots were usually slightly astigmatic, with the better HOEs having astigmatic differences of ~1-2 mm. The CCD imaging system software had provisions to calculate the encircled energy as a fraction of the total energy falling on the detector (after a background subtraction) for any size circle or ellipse drawn on the image (Fig. 9). For round looking spots, we found the circle, centered on the energy centroid of the focal spot, that contained about 86.5% of the total energy. If the focal spot resembled an ellipse, then the FWHM and $1/e^2$ points were measured for each axis of the ellipse. The encircled energy versus the diameter of such focal plane apertures are plotted for HOEs #1R and 2 in Figs. 10 & 11.

It may seem that by using float glass in the construction of the HOEs that the focal spot sizes would be limited by the aberrations induced from the glass. However, the performance is limited by random non-uniformities in the bulk index of the gelatin induced by non-uniformities in the chemical processing used to create the index modulation. The process liquids always leave a trail

behind as they run off the film following removal from the processing vats. At the surface of the gel these trails are seen as very small surface deformations. Each low spot has under it a higher density of gel than each high spot, so that optical path thickness is constant. Thus, planar wave fronts are not distorted due to refraction by the uneven surface. If a substance with uniform density, like epoxy, is applied to that surface and allowed to fill in all those low spots so that the exit surface is now level, then the time to transit from the bottom of a low spot to the new exit surface has been increased relative to the time to transit from a nearby high spot to the same surface. The result is refraction-induced distortions in beam steering. This effect is believed to be the current major source of wavefront errors introduced in light diffracted by the HOE or grating. It typically introduces between 100 and 200 μrad of aberration to the wavefronts.

To minimize this effect in gelatin the processing needs to be improved so that it is more uniform and creates fewer high and low density regions with associated high and low elevations at the surface as well as other volumetric distortions of the fringe structure. Then a cover glass or a layer of epoxy will not create spot enlargement and we expect to see 50 μrad spots, even with a wave or two of error in the recording optics and cover glass.

Other sources of wavefront errors include residual spherical aberration and astigmatism not completely corrected in the exposure optical design.

Prototype Lidar Systems based on HOE telescopes

We designed and constructed a simple lidar to test the concept of a scanning holographic telescope system based on the green reflection HOE #1R. The HOE is the disk at the far end of the bench at the bottom of Fig. 12. The laser transmitter (1mJ @ 532 nm, 20 pps) is the dark box located on the left, emitting a beam through a diverging lens and a beam tube to a 45-degree turning mirror that directs the beam down and normal to the center of the HOE. The HOE

collimates the laser beam while diffracting it up at a 43.5 degree angle to the vertical. At this point the beam is about 4 cm in diameter. The backscattered radiation is collected by the entire HOE aperture and focused to a 2.0 mm field stop located in the dark cylinder supported on the tripod directly above the HOE. The central portion of the HOE that is used to transmit the laser beam is obscured from the detector by the beam turning mirror mount and housing located on the assembly just above the HOE.

The HOE is mounted on a manual rotation stage in order to scan the system. A photon counting photomultiplier detector is mounted in the light colored cylinder directly above the field stop with a 10 nm interference filter between them to help cut down on stray background light. The concept was successfully tested in nighttime operation in this configuration³³.

In 1995, a motorized turntable was installed in the system and it was moved to the roof of the physics building at Western Maryland College (since renamed McDaniels College) in Westminster, Maryland. The system was dubbed PHASERS and has been the subject of undergraduate research projects²⁵.

PHASERS was relocated to Saint Anselm College in Manchester, New Hampshire in 1998 and outfitted with a sturdier structure and baffles (Fig. 3). It continues to be used to introduce undergraduates to the field of lidar remote sensing.

The second lidar to use a scanning HOE telescope is HARLIE. HARLIE is a technology demonstration to test the utility of using holographic scanning receivers in lidar systems at the 1064 nm Nd:YAG wavelength and in an aircraft environment. Built as an aerosol backscatter lidar system, HARLIE uses a 40 cm diameter by 1 cm thick transmission HOE as the laser collimating optic as well as the receiver primary optic. It has a 45 degree diffraction angle and a 1 meter focal length normal to its surface. It rotates continuously at rates up to 30 rpm, and can

also operate in step and stare or static modes. Improvements to the HOE design and manufacturing enabled us to obtain a 160 μ rad focal spot encircling 86.5% of the diffracted energy. The higher angular resolution greatly improved daytime performance over PHASERS. The focus is placed on a 200 μ m, 0.22 NA fiber optic field stop that delivers the backscattered light to the aft optics package. The aft optics contains a collimating lens, a 500 pm interference filter, a focusing lens, and a Geiger-mode avalanche photodiode. The Q-switched transmitter is a CW-pumped Nd:YAG laser capable of delivering over 20 w output, pulsed or CW. In HARLIE we run it at a 5 KHz repetition rate with 400 μ J pulse energy. The beam is expanded using a -61 mm f. l. lens before being transmitted through the center of the HOE, which collimates the beam to 70 μ rad divergence x 20 mm diameter. The angular extent of the transmitted beam is smaller than the full-aperture FOV because the small portion of the HOE illuminated by the outgoing laser beam introduces fewer wavefront errors.

Figure 14 is a photograph of the HARLIE transceiver assembly mounted on its transportation dolly and electronics rack. The lidar can also operate on the ground with the transceiver directed in any of 8 elevation positions spaced 45° apart. In this figure the system is pointed up, so the HOE appears on top, mounted in a large ring gear and ball bearing assembly. The laser is mounted on the bottom and the beam is directed into the box and onto the HOE rotation axis, exiting through the center of the HOE. The electronics rack contains the data system, the laser power supply and chiller, the scan motor controller, a GPS receiver, and an aircraft inertial navigation system interface. The entire transmitter/receiver package can be placed within centimeters of an aircraft instrument window. A 52 cm clear aperture window allows for an unobstructed view in all directions around the conical scan (Fig. 15).

Figure 16 is a sample of ground-based data taken with HARLIE in the scanning mode. The conical surface of the HARLIE scan is projected in an isometric view out to 5 km altitude and horizontal range. Increasing levels of backscatter are revealed as darker shades of gray. There is a thin stratus cloud layer at 2 km altitude and multiple thicker cloud layers between 3 and 5 km altitude, with virga streaming from the layer near 4 km altitude in the lower right hand portion of the cone. This single 36-second scan of data was taken on 9 June 1999 at Saint Anselm College in Manchester, New Hampshire during the HOLO-2 campaign^{34, 35}. It reveals the rich details and atmospheric aerosol structures that a scanning lidar system is capable of detecting. Sequential series of such scans can be analyzed for aerosol and cloud motions that can be used to infer atmospheric wind vectors^{36, 37}. Examples of time-lapse visualizations and other HARLIE data are available on the HARLIE web site³⁸.

Practical Considerations

After extensive testing and field use of various configurations of holographic gratings and HOEs for lidar applications as the primary transceiver optic, we have some additional insights into what works and what doesn't work, and what may work better with improvements in design and construction.

Note that with either HOE type the collimated beam cross-sectional area (transmitted and received) is an ellipse, with the effective lidar receiver collection area reduced from the actual HOE area by the cosine of the diffraction angle.

We have found that the HOEs constructed in the manner described in Section 3 work without any ill effects when used with moderate power, low energy Q-switched lasers. The HARLIE laser typically produces 50 nsec, 400 μJ pulses at 5 KHz rep-rate, and illuminates the central 2 cm diameter of the HOE for an average energy density of 130 $\mu\text{J}/\text{cm}^2$ and average power density

of 640 mW/ cm^2 . Similarly, the green PHASERS laser (1 mJ, 20 ns, 2 kHz) has been used without any apparent degradation in the HOE performance over time. Even several years in an uncontrolled (but enclosed) environment and many hours of exposure to direct sunlight have not had any noticeable effect on its performance. However, when a small holographic grating was illuminated with the unexpanded output of a large pulse (600 mJ, 10 nsec) of a 532 nm Q-switched Nd:YAG laser having an energy density of $\sim 1 \text{ J/cm}^2$, the absorption from the traces of residual dichromate and the epoxy used to encapsulate the HOE with a cover glass was sufficient to cause catastrophic optical damage.

Boresight alignment between the laser and the HOE is essentially the same as for a lidar using a conventional telescope. For a coaxial or parallel transmitter-receiver alignment, one wishes to make the laser appear to emanate from the field stop when viewed looking back into the lidar from infinity. If the field stop is not positioned exactly on the rotation axis, the scan will still describe a cone, but the axis will be tilted with respect to the HOE rotation axis according to Eq. 3.

One expects to have some polarization dependence of the diffraction efficiency in an HOE. In order to match the diffraction efficiency of *s* and *p* polarized light, one needs to control the average index and the index modulation values during the HOE manufacturing process³⁸. One has to sacrifice peak efficiency for either polarization in order to achieve equal polarization at the design wavelength and diffraction angle. The point at where both polarizations are equal is about 85%. It is very difficult to control the manufacturing process parameters accurately enough to exactly match the efficiency for both polarizations. Typically there will be a few-percent difference between them. And because the diffraction angles vary over the surface of the HOE, there is a modest dependence of the diffraction efficiency over different areas of the HOE. Using

a linearly polarized laser, we have found the transmitted laser energy for the HARLIE HOE to vary with scan angle in a sinusoidal fashion by 5 % peak-to-peak, at half the scan period. This effect is minimized by circularizing the polarization of the laser transmitter.

Gelatin is an elastic material and conforms to any substrate to which it is applied. When the substrate changes size due to temperature changes, the holographic film will follow. The primary effect is a change in the surface grating pitch on each surface of the film. This surface grating is what determines the optical geometry, *i.e.* the focal length and the diffraction angle will both change in direct proportion to the expansion rate of the substrate. A typical thermal expansion coefficient for glass of $\sim 10^{-5}$ yields a change in diffracted angle of about $\sim 15 \mu\text{rad/K}$ and a change in focal length of $\sim 10 \mu\text{m/K}$ for the HOEs we used in our lidars. The latter is of little consequence given the depth of field of an $f/2.5$ lens. The diffraction angle change will basically change the cone angle of the scan pattern. As long as the transmitter and receiver field stops are built with an athermal mechanical design, boresight alignment should not be detrimentally affected. Barring any large thermal gradients across the HOE optic, the transmitted beam and the receiver FOV should track together.

We also experimented with using holographic transmission plane gratings placed in front of a conventional telescope to generate the conical scan. This technique has one disadvantage over using an HOE to perform the scanning if the grating is also used to transmit the outgoing laser beam. The $\sim 2\text{-}5\%$ of undiffracted zero-order light constitutes a second collimated transmitted beam which will generate its own return signal that will be collected and combined with the main return signal from the $+1$ diffracted order (Figure 17a). On its return, the backscattered light does not meet the Bragg condition for diffraction in the grating and passes through relatively unattenuated. If there are any clouds in the beam path, their backscatter signals may be

comparable in magnitude to that of cloud-free regions and will be superimposed on the first order diffracted beam signal. To make matters worse, the two signals will have a different range-altitude relationship depending on the pointing direction and orientation of the lidar. This problem can be alleviated by using a baffle tube for transmitting the beam after it leaves the grating. However, this baffle will have to be attached to the rotating optic in order to steer with the laser beam, adding to the mechanical complexity of the system.

This “cross-talk” is not a problem in the HOE based telescope. The zero-order transmitted beam continues to diverge after leaving the HOE. Atmospheric backscattered light from the 0-order transmitted beam fails to match the Bragg condition and is not diffracted to a focus in the telescope (Fig. 17b). It is also best to use a design in which second order is evanescent. For an HOE in which the focal side axis is normal to the optic, then the collimated side diffraction angle should be 30 degrees or more to eliminate higher diffraction orders.

That any given HOE is effective only over a limited spectral band opens the possibility of wavelength multiplexing HOEs using various approaches. One can make a sandwich of individual HOEs, each diffracting its own specific wavelength while being transparent to the other wavelengths. Also, one can produce multiple holograms in a single film using multiple exposures. Alternatively, multiple HOEs may occupy separate areas of the substrate, although that would not make efficient use of the available aperture. In order to accomplish the focusing of different wavelengths to separate detectors that remain stationary as the HOE is rotated, the foci may be placed at different locations along the rotation axis, delivering light to optical fibers which will carry the light to detectors located elsewhere (Fig. 18a). Alternatively, the foci may be arranged off-axis at various locations in the focal plane of a grating/HOE system in which the functions of scanning and focusing reside in separate optics (Fig. 18b). Further reductions in

cross-talk are possible by offsetting the diffraction plane of each HOE in azimuth angle. This is also a technique for angle multiplexing several HOEs for use at the same wavelength^{30, 31}.

Special consideration must be given to multiplexing HOEs for simultaneously diffracting laser harmonic wavelengths, as the m th order of the m th harmonic will diffract efficiently in the same direction as the first order of the fundamental wavelength for any given HOE. For example if one wished to utilize the 1st and 3rd harmonics of a Nd:YAG laser and have the HOE diffract each of the wavelengths to separate detectors, one might use the design in Fig. 19. A reflection HOE designed to diffract 355 nm light is placed on top of a transmission HOE designed for 1064 nm light. The fringes of the UV HOE are too close together to create constructive interference at 1064 nm, hence the IR radiation will pass through to the transmission HOE underneath and be focused on the opposite side of the assembly.

For observing different wavelengths that are close enough to fall within the diffractive bandwidth of the HOE, the foci will fall along a line at an angle to the HOE, with different wavelengths having focal distances inversely proportional to their wavelength. The spectrum will rotate with the HOE, defeating one of the biggest advantages of using the HOE, to simplify the scanning design. In order to capture this spectrum while rotating, a line of detectors or focal plane optics must rotate at the same rate. Berkoff et. al.²⁹ reported on an experimental Raman lidar design to capture the elastic backscatter and three Raman scattered wavelengths, using the HOE as both a telescope and a spectrograph.

Summary and Conclusions

We have shown that large HOEs can be used effectively as conical scanning lidar telescopes which are mechanically much simpler and more compact than designs using conventional telescopes and scan optics. When an HOE is made with a point source object beam diverging and

normal to the film, and a collimated reference beam at some angle to the film, the object beam defines the focal length and the rotation axis for scanning, while the reference beam defines the scan cone half-angle. A conical scan pattern is generated when the HOE is rotated in its own plane about the optic axis that goes through the focal point. Low energy density laser pulses can be transmitted through the HOE, which acts as the final collimating and beam steering optic. Two prototype lidar systems, one using a reflection HOE with a 532 nm laser transmitter, and one using a transmission HOE with a 1064 nm laser transmitter have been built and successfully tested. Angular resolutions as small as 160 μ rad have been obtained, allowing HOEs to be used as small FOV receivers. Holographic plane gratings can also be used to conically scan conventional telescopes or static HOEs provided care is taken to suppress possible zero and negative first order diffracted light if the grating is used to also scan the outgoing laser beam. Several years of use have shown the HOE assemblies to be robust and reliable. Future developments include scaling to meter apertures and larger, increasing angular resolution, and multiplexing HOEs to utilize multiple wavelengths or multiple fields of view so as to negate the need to move the HOE in order to scan.

Acknowledgements

The authors wish to thank the following programs and offices for their support of this research: The NASA Goddard Director's Discretionary Fund, Donald Friedman and Nancy McClennan of the NASA SBIR program office, Nona Cheeks, Joseph Famiglietti, and Anel Flores of the NASA Goddard Technology Commercialization Office, Lisa Callahan of the NASA Cross-Enterprise Program, and Steve Mango of the Integrated Program Office. We thank Barry Coyle for helping to design and build the first laser for PHASERS, Steve Palm for developing the first PHASERS data acquisition software, Kurt Medine, Wayne Welch, and Jeffrey Freemire for



PHASERS mechanical design support, Alex Leung for HOE testing, Orbital Sciences Corporation and Science and Engineering Services, Inc. for HARLIE engineering, fabrication, and HOE testing. Special thanks go to David Miller for his help deploying and operating HARLIE and to Sangwoo Lee for help in analyzing the HOE test data.

References

1. G. K. Schwemmer and T. D. Wilkerson, "Holographic Optical Elements as Conically Scanned Lidar Telescopes," in *Optical Remote Sensing of the Atmosphere*, Vol. 18 of Tech. Digest Series, (Optical Society of America, Wash. D. C., 1991), pp. 310-312.
2. G. Schwemmer, "Conically Scanned Holographic Lidar Telescope," *United States Patent* #5,255,065, issued Oct. 19, 1993.
3. G. Schwemmer, T. Wilkerson, and D. Guerra, "Compact scanning lidar systems using holographic optics," in *Optical Remote Sensing for Industry and Environmental Monitoring*, Proc. SPIE **3504**, 51-59 (1998).
4. G. Schwemmer, D. Miller, T. Wilkerson, D. Guerra, and R. Rallison, "NASA lidar uses HOEs for lightweight scanning," *Laser Focus World*, **38**, No. 6, pp. 141-147, June 2002.
5. N. Takeuchi, H. Shimizu, Y. Sasan, and N. Sugimoto, "LAMP lidar for wide-area air pollution monitoring," in *Conf. Abstracts, 10th International Laser Radar Conf.*, Oct. 6-9, 1980, Silver Spring, MD, p. 16-17.
6. D. Morancais, R. Sesselmann, G. Benedetti-Michelangeli, and M. Hueber, "The Atmospheric Lidar Instrument (ATLID)," *Acta Astronautica*, **34**, 63-67 (1994).
7. D.N. Whiteman, S.H. Melfi, and R.A. Ferrare, "Raman lidar system for the measurement of water vapor and aerosols in the earth's atmosphere," *Appl. Opt.*, **31**, 3068-3082 (1992)

8. E. E. Uthe, N. B. Nielsen, and T. E. Osberg, "Airborne scanning lidar observations of aircraft contrails and cirrus clouds during SUCCESS," *Geophys. Res. Lett.*, **25**, 1339-1342 (1998).
9. P. A. Hwang, W. B. Krabill, W. Wright, R. N. Swift, E. J. Walsh, "Airborne scanning lidar measurement of ocean waves, *Remote Sensing of Environment*, **73**, 236-246 (2000).
10. S. P. Palm, S.H. Melfi and D. L. Carter, "New airborne scanning lidar system: applications for atmospheric remote sensing, *Appl. Opt.*, **33**, 5674-5681 (1994).
11. J. L. Irish and W. J. Lillycrop, "Scanning laser mapping of the coastal zone: the SHOALS system," *ISPRS J. of Photogramm. & Remote Sensing*, **54**, 123-129 (1999).
12. J. G. Hawley, R. Targ, S. W. Henderson, C. P. Hale, M. H. Kavaya, and D. Moerder, "Coherent launch-site atmospheric wind sounder: theory and experiment," *Appl. Opt.*, **32**, 4557-4568 (1993).
13. M. Bennett, S. Sutton, and D. R. C. Gardiner, "Measurements of wind speed and plume rise with a rapid-scanning Lidar," *Atmos. Environ.*, **26A**, 1675-1688 (1992).
14. C. Werner, P. H. Flamant, O. Reitebuch, F. Kopp, J. Streicher, S. Rahm, E. Nagel, M. Klier, H. Herrmann, C. Loth, P. Delville, P. Drobinski, B. Romand, C. Boitel, D. Oh, M. Lopez, M. Meissonnier, D. Bruneau, A. Dabas, "Wind infrared Doppler lidar instrument," *Opt. Eng.* **40**, 115-125 (2001).
15. [REDACTED], "The Multi-center Airborne Coherent Atmospheric Wind Sensor," *Bull. Amer. Meteor. Soc.*, **79**, 580-598 (1998).
16. E. W. Eloranta and D. K. Forrest, "Volume imaging lidar of the convective structure surrounding the flight path measuring aircraft," *J. Geophys. Res.*, **97**, 18,383-18,393 (1992).
17. W. P. Hooper and L. U. Martin, "Scanning lidar measurements of surf-zone aerosol generation," *Opt. Eng.*, **38**, 250-255 (1999).

18. W. E. Eichinger, D. I. Cooper, P. R. Forman, J. Griegos, M. A. Osborn, D. Richter, L. L. Tellier, and R. Thornton, "The development of a scanning Raman water vapor lidar for boundary layer and tropospheric observations," *J. of Atmos. Oceanic Technol.*, **16**, 1753-1766 (1999).
19. B. M. Gentry, H. L. Chen, S. X. Li, "Wind measurements with 355-nm molecular Doppler lidar," *Opt. Lett.* **25** (17), 1231-1233 (2000).
20. Y. D. Chen and J. Ni, "Dynamic calibration and compensation of a 3-D laser radar scanning system," *IEEE Trans. Robotics Automat.*, **9**, 318-323 (1993).
21. J. B. Blair, D. L. Rabine, and M. A. Hofton, "The laser vegetation imaging sensor: a medium-altitude, digitisation-only, airborne laser altimeter for mapping vegetation and topography," *ISPRS J. of Photogrammetry and Remote Sensing*, **54**, 115-122 (1999).
22. D. H. Close, "Optically recorded holographic optical elements," in *Handbook of Optical Holography*, H. J. Caulfield, Ed., (Academic Press, Inc.1979), pp.573-585
23. R. D. Rallison, "Holographic optical elements (HOEs) in dichromated gelatin (DCG):
• progress," in *Applications of Holography*, L. Huff, Ed. *Proc. SPIE* **523**, 292-295 (1985).
24. C. Gilbreath, A. E. Clement, and J. W. Wagner, "Holographic Optical Elements which diffract efficiently in the near-infrared for operation with laser diodes for spacecraft communications," in *Practical Holography III*, T. H. Jeong, Ed. *Proc. SPIE* **747**, 43-50 (1987).
25. D. V. Guerra, A. D. Wooten, Jr., S. S. Chaudhuri, G. K. Schwemmer, and T. D. Wilkerson, "Prototype Holographic Atmospheric Scanner for Environmental Remote Sensing ", *J. of Geophysical Research*, **104**, No. D18, 22,287-22,292 (1999).

26. R. D. Rallison and S. R. Schicker, "Wavelength compensation by time reverse ray tracing,"  Proc. SPIE, **2404**, p. 217 (1995).
27. R. D. Rallison and S. M. Arnold, "Wavelength compensation at 1.064 μ using hybrid optics," in *Diffraction and Holographic Optics Technology III*, I. Cindrich, S. A. Benton, Eds., Proc. SPIE, **2689**, 217-226 (1995).
28. G. K. Schwemmer, "Holographic airborne rotating lidar instrument experiment," *19th International Laser Radar Conference*, U. Singh, S. Ismail, G. K. Schwemmer, Eds. (NASA/CP-1998-207671/PT2, NASA, 1998), pp. 623-626.
29. T. A. Berkoff, D. N. Whiteman, R. D. Rallison, G. K. Schwemmer, L. Ramos-Izquierdo, and H. Plotkin, "Remote detection of Raman scattering by use of a holographic optical element as a dispersive telescope", Optics Letters, **25**, 1201-1203 (2000).
30. G. K. Schwemmer, "Shared-aperture multiplexed holographic scanning telescopes," Photonics Tech Briefs, **25**, No. 7, p. 18a, July 2001
31. G. K. Schwemmer, "Methods and systems for collecting data from multiple fields of view," U. S. Patent No. 6,479,808, awarded Nov. 12, 2002, .
32. H. Kogelnick, Bell Syst. Tech. J. **48**, 2909-2947 (1969).
33. G. K. Schwemmer and T. Wilkerson, "Development of a holographic telescope for optical remote sensing," in *Spin-Off Technologies from NASA for Commercial Sensors and Scientific Applications*,  Proc. SPIE, **2270**, 40-47 (1994).
34. T. D. Wilkerson, J.A. Sanders, I.Q. Andrus, G.K. Schwemmer, D.O. Miller, D. Guerra, J. Schnick, and S.E. Moody, "The HOLO series: critical ground-based demonstrations of holographic scanning lidars", in *2nd Asia-Pacific Symposium on Remote Sensing*, U. N. Singh, T. Itabe, N. Sugimoto, eds., Proc. SPIE, **4153**, 63-69 (2001).

35. G. K. Schwemmer, T. D. Wilkerson, J. A. Sanders, D. V. Guerra, D. O. Miller, S. E. Moody, "Ground based operational testing of holographic scanning lidars," in *Advances in Laser Remote Sensing*, A. Dabas, C. Loth and J. Pelon, eds., (Ecole Polytechnique, publisher, France, 2001), pp. 69-72.
36. J. A. Sanders, T. D. Wilkerson, G. K. Schwemmer, D. O. Miller, D. Guerra, S. E. Moody, "Comparison of two lidar methods of wind measurement by cloud tracking," presented at the 20th International Laser Radar Conference, Vichy, France, 10-14 July 2000.
37. T. D. Wilkerson, I. Q. Andrus, G. K. Schwemmer, D. O. Miller, "Horizontal Wind Measurements using the HARLIE Holographic Lidar", in *Optical Remote Sensing for Industry and Environment Monitoring II*, U. N. Singh, ed., Proc. of SPIE, **4484**, 64-73 (2002). <http://harlie.gsfc.nasa.gov/>.
39. R. D. Rallison and S. R. Schicker, "Polarization properties of gelatin holograms," in [REDACTED] Proc. SPIE, **1667**, 266-275 (1992).

Figures

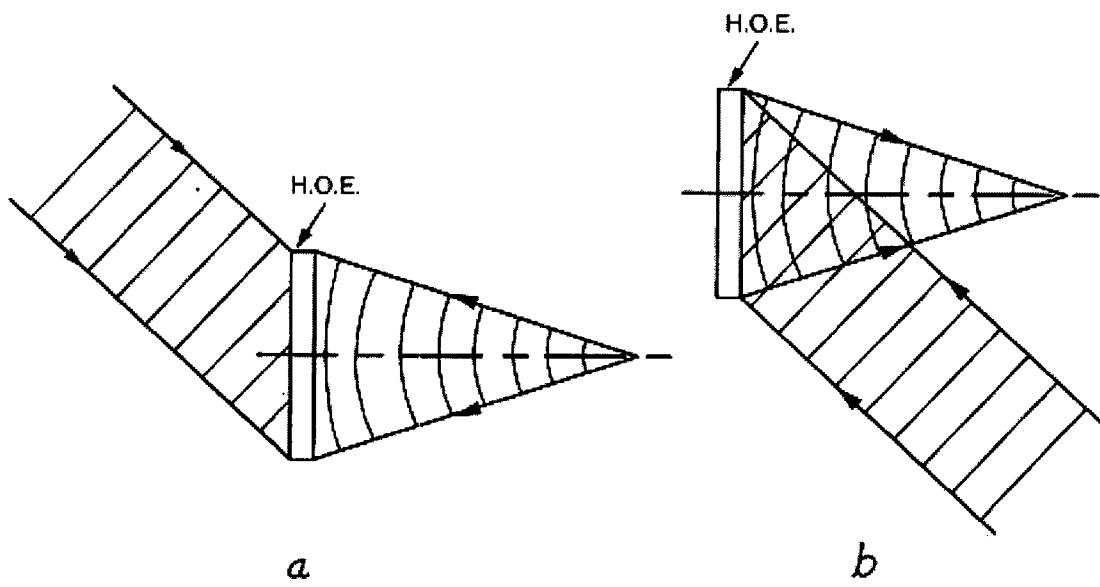


Fig. 1. Exposure geometry (a), and reconstruction geometry (b) for a reflection HOE.

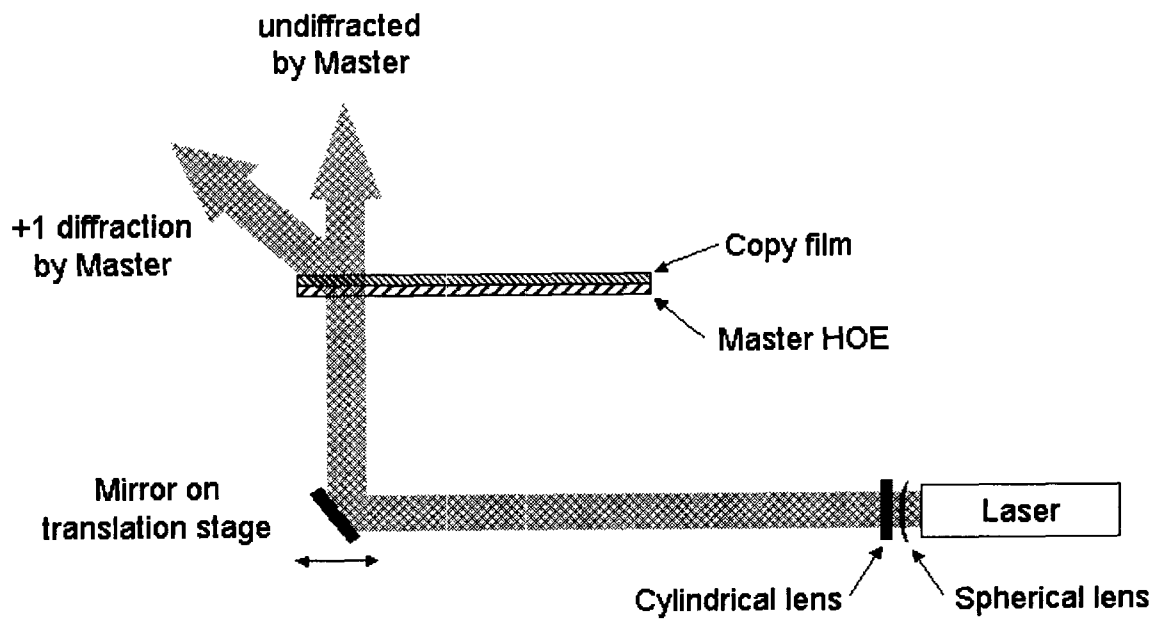


Fig. 2. Copying an HOE from a master. The laser beam is formed into a sheet (long dimension is into the paper) before scanning the master/copy assembly.



Fig. 3. Photograph of several HOEs and holographic gratings designed for lidar applications.

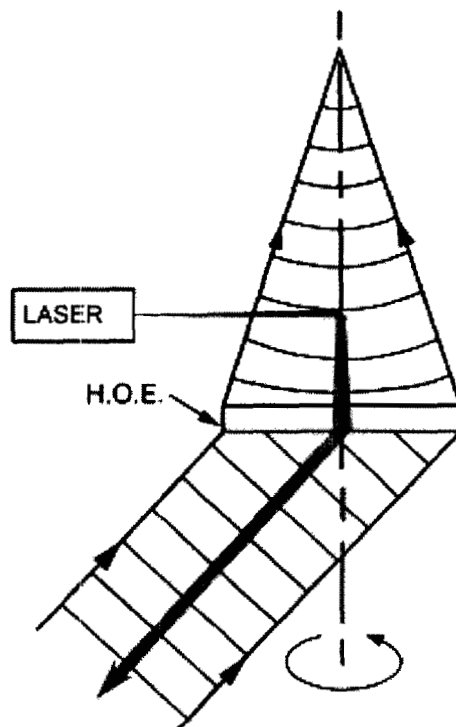


Fig. 4. Geometry for using a transmission HOE to scan the transmitted laser as well as the receiver FOV.

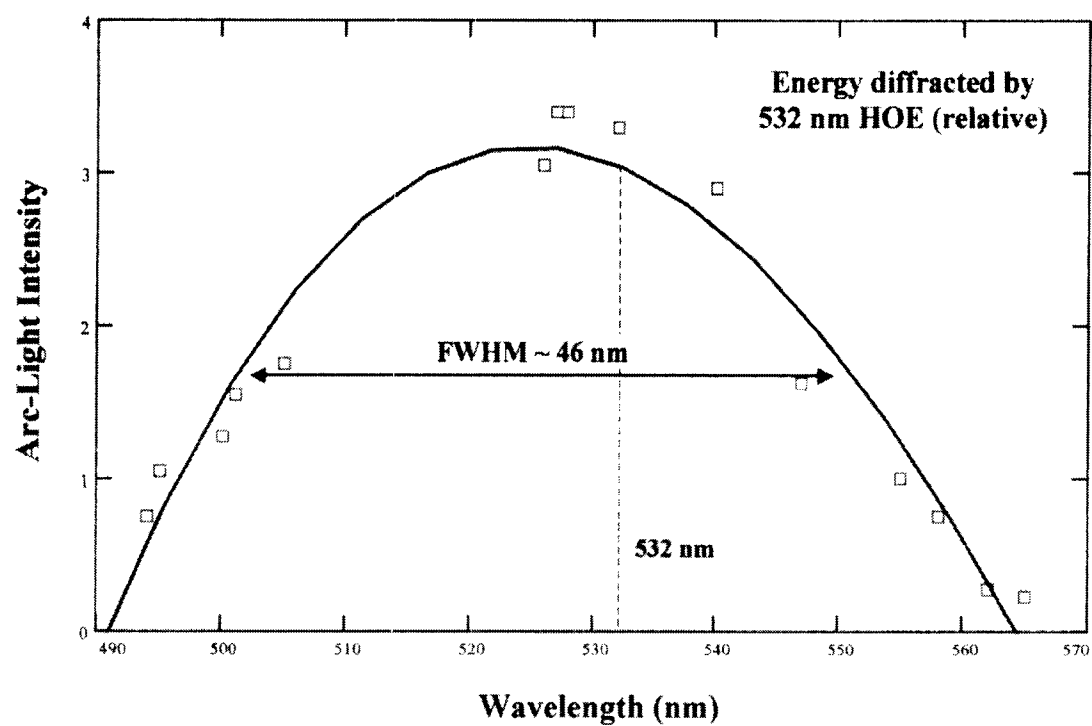


Fig. 5. Relative spectral response of HOE #1R. The curve is a spline fit to the data points.

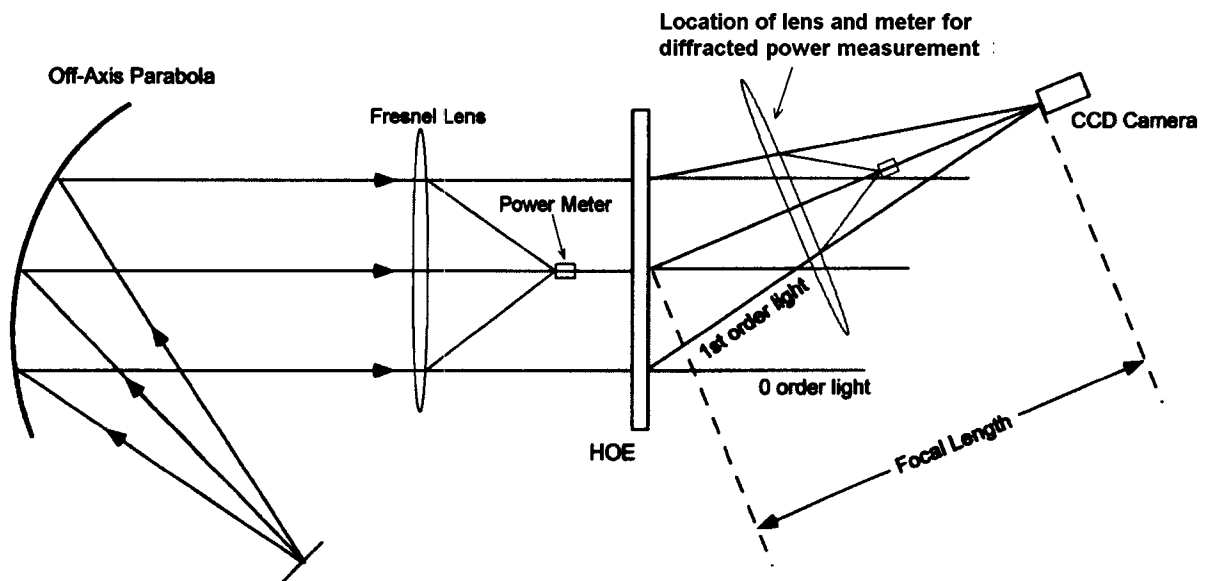


Fig. 6. Setup for measuring diffraction efficiency and spot size.

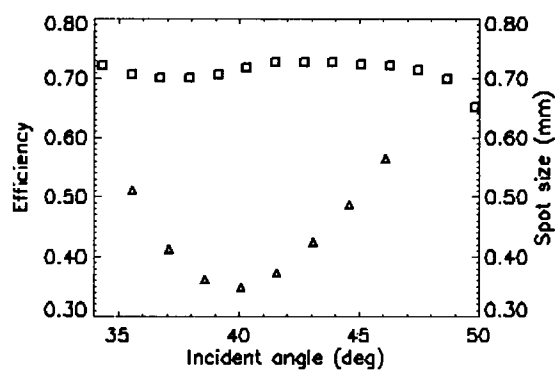


Fig. 7. Diffraction efficiency (squares) and spot size (triangles) as a function of incident angle for HOE#7R.

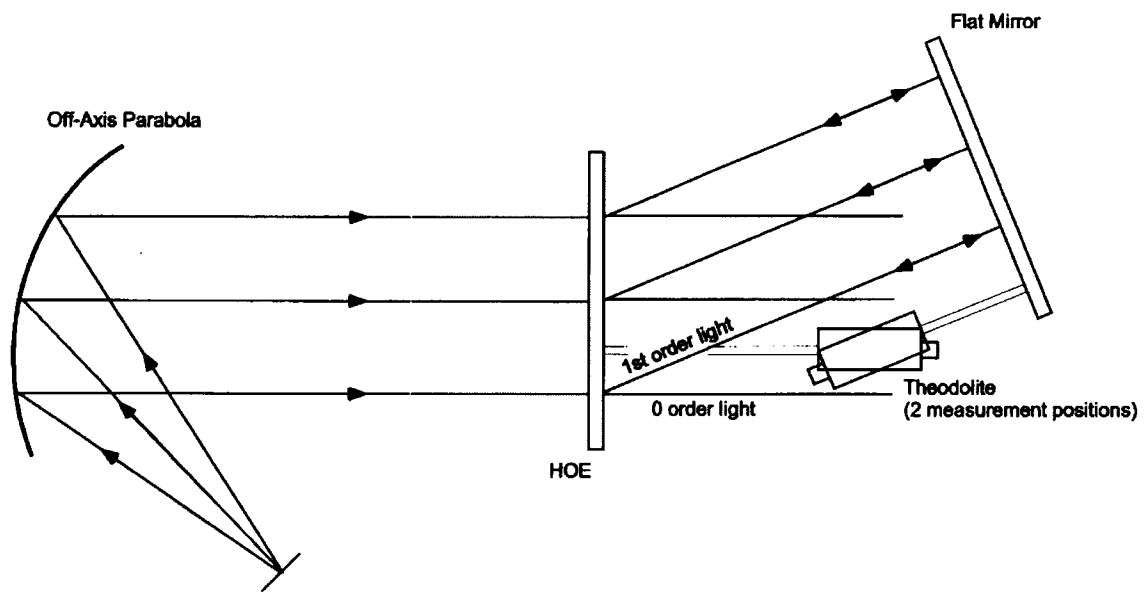


Fig. 8. Grating diffraction angle test setup.

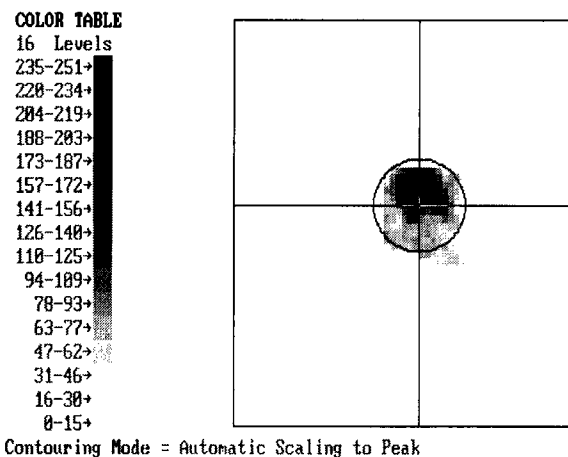


Fig. 9. CCD camera image of focal spot of one of the preliminary copies of HOE #2. The reticle circle diameter is 270 μm .

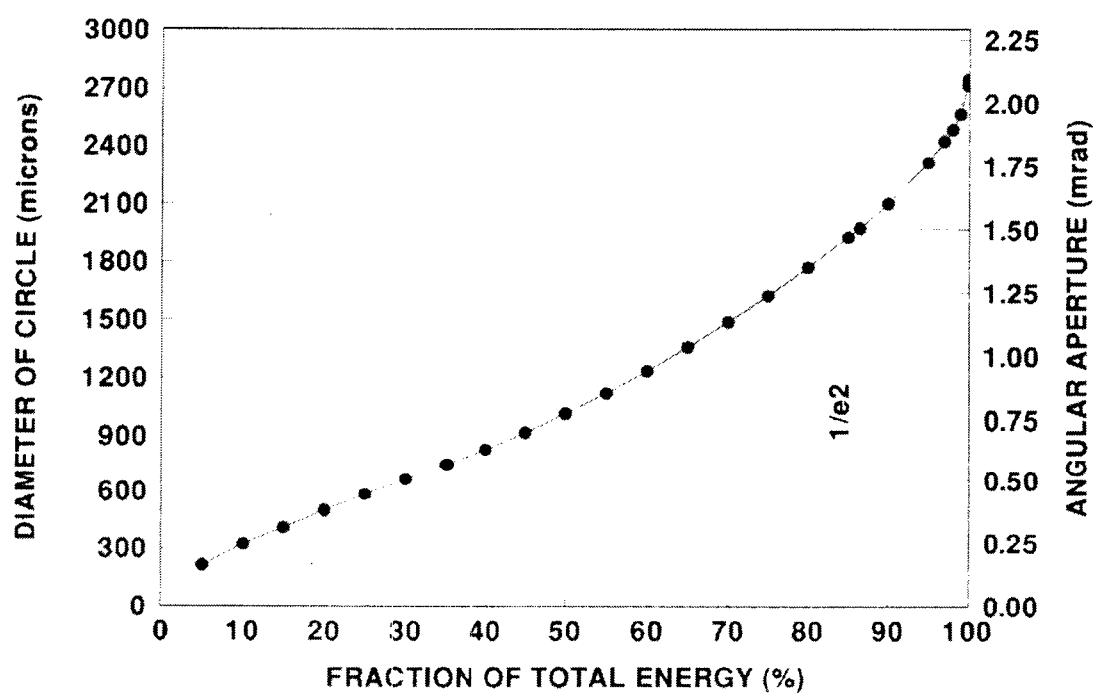


Fig. 10. Encircled energy function of focal spot for HOE #1R.

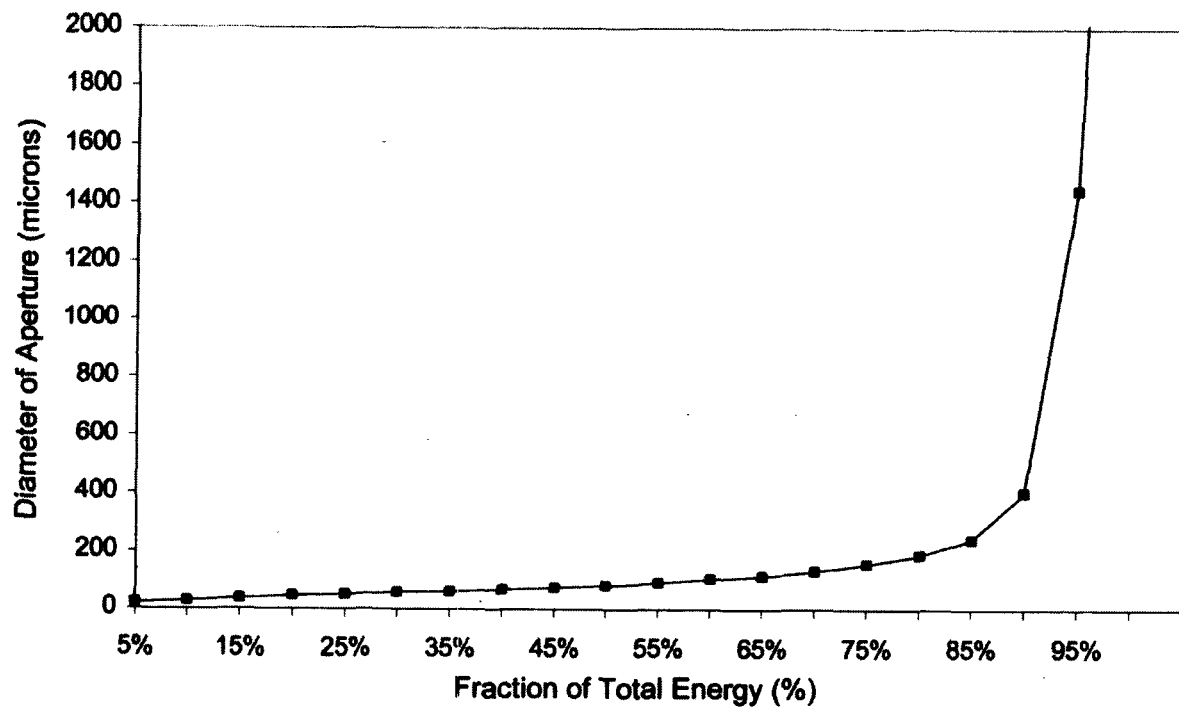


Fig. 11. Encircled energy function for HOE #2.

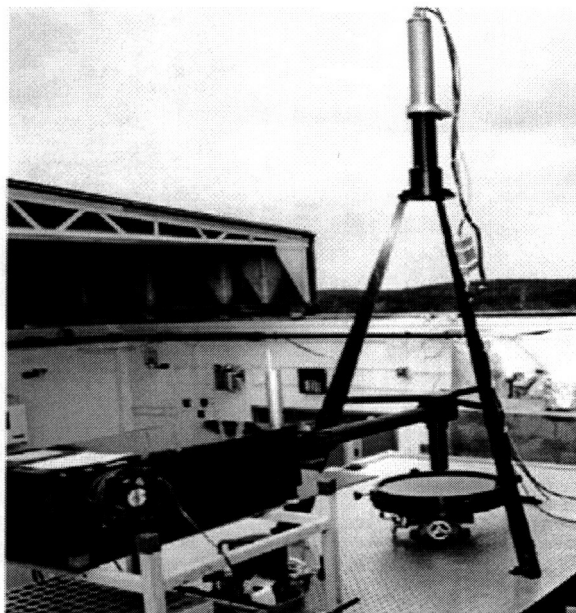
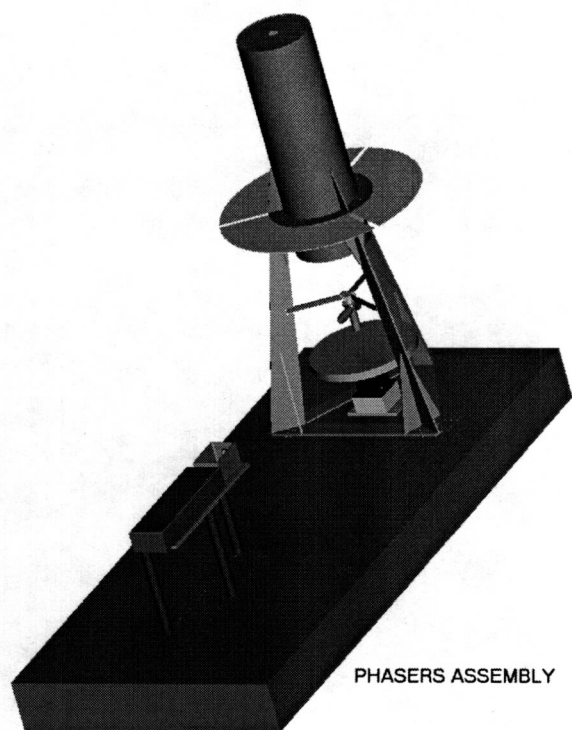


Fig. 12. Early version of the first atmospheric lidar using a scanning reflection HOE.



PHASERS ASSEMBLY

Fig. 13. Mechanical drawing of the new PHASERS transceiver.



Fig. 14. HARLIE system transceiver (left) and data system (right).

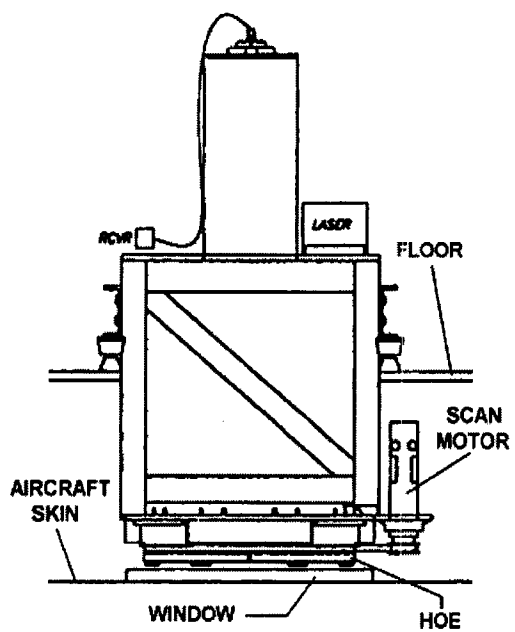


Fig. 15. Position of HARLIE in an aircraft, suspended from the floor.

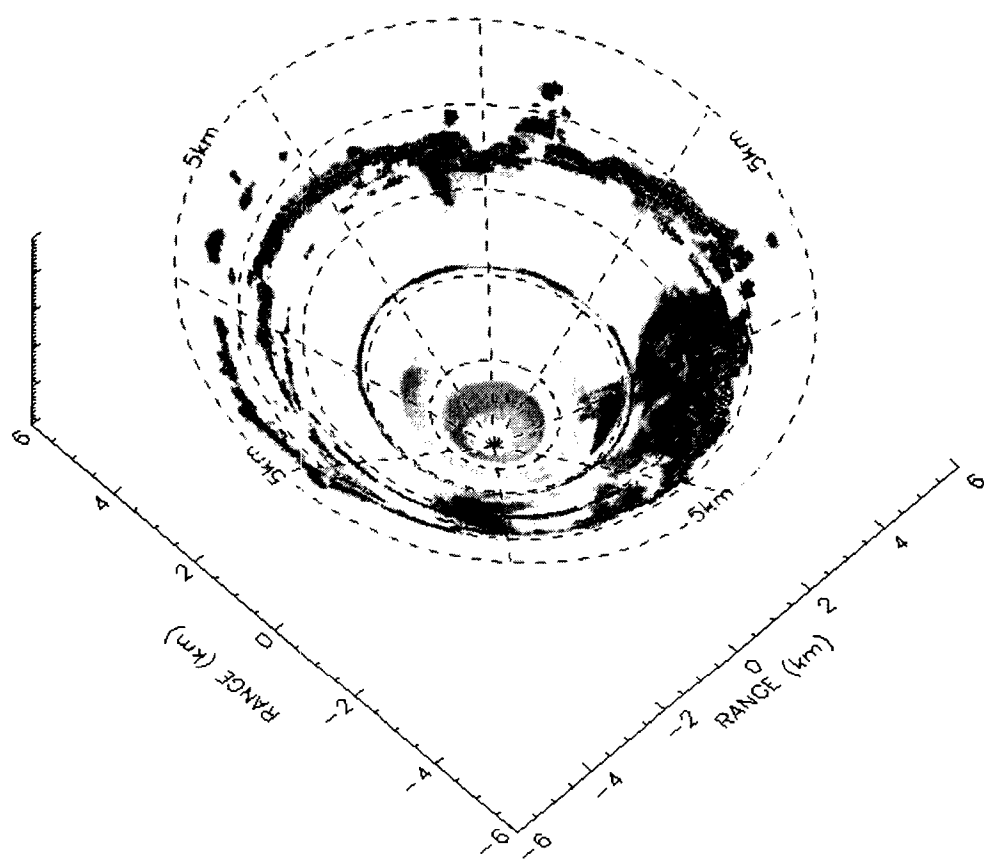


Fig. 16. A scan of ground-based HARLIE backscatter data taken the night of 9 June 1999, during the HOLO-2 campaign (Wilkerson et.al., 2001).

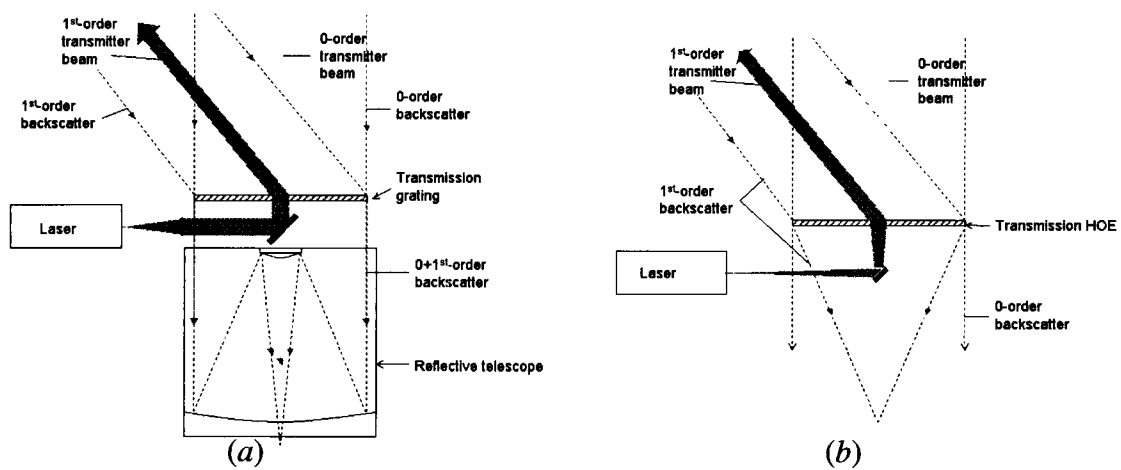


Fig. 17. a) Crosstalk from the 0-order beam is focused in a conventional telescope used with a grating scanner. b) Crosstalk from the 0-order beam is not focused in an HOE telescope.

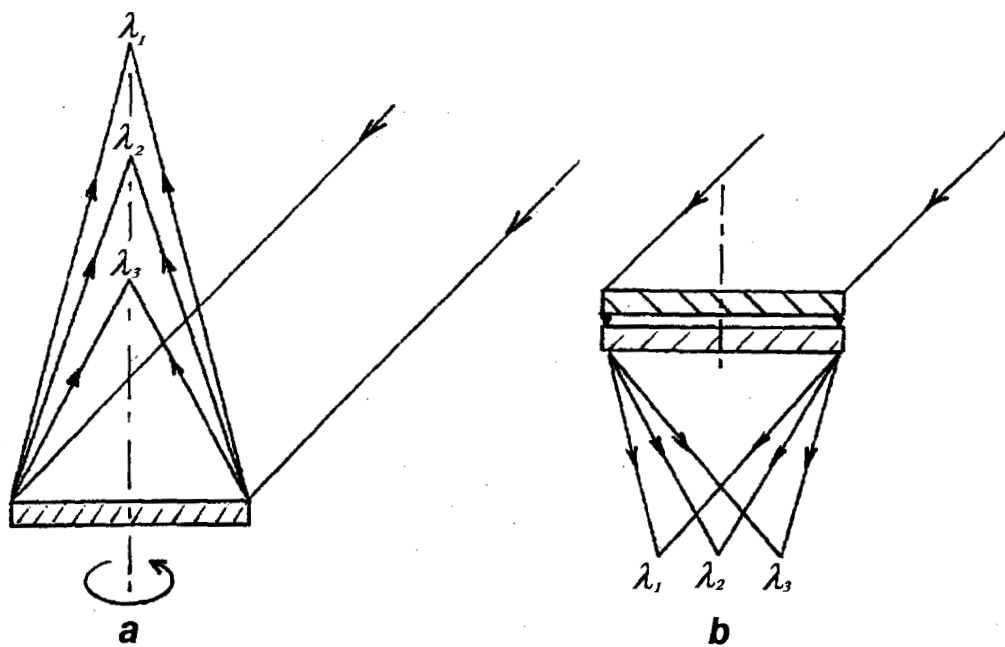


Figure 18. Two methods of wavelength multiplexing HOEs to maintain static detector assemblies. a) The foci are all placed on the rotation axis. b) A rotating plane grating scanner followed by a static multiplexed HOE.

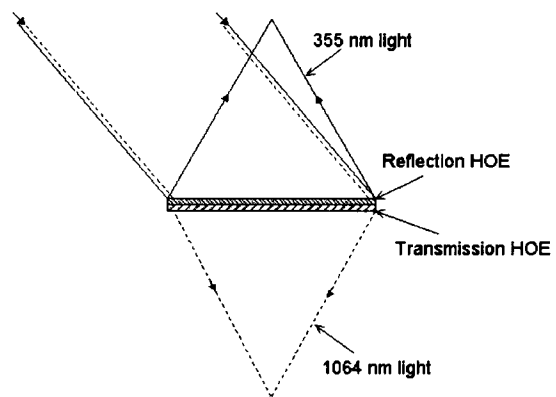


Fig. 19. Wavelength multiplexed design concept using a 355 nm reflection HOE on top of a 1064 nm reflection HOE.

Figure Captions

Fig. 1. Exposure geometry (*a*), and reconstruction geometry (*b*) for a reflection HOE.

Fig. 2. Copying an HOE from a master. The laser beam is formed into a sheet (long dimension is into the paper) before scanning the master/copy assembly.

Fig. 3. Photograph of several HOEs and holographic gratings designed for lidar applications.

Fig. 4. Geometry for using a transmission HOE to scan the transmitted laser as well as the receiver FOV.

Fig. 5. Relative spectral response of HOE #1R. The curve is a spline fit to the data points.

Fig. 6. Setup for measuring diffraction efficiency and spot size.

Fig. 7. Diffraction efficiency (squares) and spot size (triangles) as a function of incident angle for HOE#7R.

Fig. 8. Grating diffraction angle test setup.

Fig. 9. CCD camera image of focal spot of one of the preliminary copies of HOE #2. The reticle circle diameter is 270 μm .

Fig. 10. Encircled energy function of focal spot for HOE #1R.

Fig. 11. Encircled energy function for HOE #2.

Fig. 12. Early version of the first atmospheric lidar using a scanning reflection HOE.

Fig. 13. Mechanical drawing of the new PHASERS transceiver.

Fig. 14. HARLIE system transceiver (left) and data system (right).

Fig. 15. Position of HARLIE in an aircraft, suspended from the floor.

Fig. 16. A scan of ground-based HARLIE backscatter data taken the night of 9 June 1999, during the HOLO-2 campaign (Wilkerson et.al., 2001).

Fig. 17. *a*) Crosstalk from the 0-order beam is focused in a conventional telescope used with a grating scanner. *b*) Crosstalk from the 0-order beam is not focused in an HOE telescope.

Fig. 18. Two methods of wavelength multiplexing HOEs to maintain static detector assemblies. *a*) The foci are all placed on the rotation axis. *b*) A rotating plane grating scanner followed by a static multiplexed HOE.

Fig. 19. Wavelength multiplexed design concept using a 355 nm reflection HOE on top of a 1064 nm reflection HOE.

Table 1

Table 1. Partial List of the HOEs and gratings manufactured and tested in this program.

Item # [†]	Wavelength (nm)	Diameter (mm)	Focal Length (mm)	Angle 1	Angle 2*
1R	532	404	1300	45	0
2	1064	404	1016	45	0
3	1064	404	∞	45	0
4	770	404	∞	45	0
5	532	404	∞	36	0
5R	532	404	1295	43	0
6a	1047	202	∞	22.5	0
6b	1047	202	760	0	22.5
7a	1047	254	∞	22.5	0
7b	1047	254	760	0	22.5

[†] An R following the number indicates a reflection hologram, otherwise it is a transmission hologram.

* For HOEs, angle 1 refers to the collimated beam axis and angle 2 refers to the focusing axis, relative a normal to the substrate.

Table 2

Table 2. Test measurement results for holographic optics of table 1.

Item #	Focal length $h \pm 2$ (mm)	Spot size $1/e^2 *$ (μrad) $\pm 5\%$	Spot size FWHM (μrad) $\pm 5\%$	Zero order efficiency $\pm 0.2 (\%)$	1 st order efficiency $\pm 2 (\%)$	Diffraction angle ± 0.1 (degrees) for smallest focal spot	Comments Errors are given column in headings unless otherwise noted.
1R	1295	1200			59	42.0 \pm 0.5	PHASERS HOE
2	1016	180		5	86	45.0	HARLIE HOE
3	N/A	N/A	N/A	9.5	73	45.0	
4	N/A	N/A	N/A	7	84	45.0	
5	N/A	N/A	N/A	13	74	36.4	
6R	1306	630	350	~3	73	40.1	~7% specular reflections from internal surfaces.
"	1306	486	269		72	40.1	The best focus occurred at this angle.
7a	N/A	N/A	N/A	1.3	91	22.8	
"	N/A	N/A	N/A	11	76	20.3	
@904nm							
7b	756.2	225 x 262	56 x 138	7.4	84	23.2	
8a	N/A	N/A	N/A	2.9	90	22.1	
8b	760.1	135 x 285	43 x 149	6.4	86.5	22.7	

* If two numbers are given they describe the major and minor axis of an ellipse, if one number it describes a circle. Either conic contains 86.5% of the energy diffracted into the first order.